Inorganic Chemistry
Article

Inorg. Chem. **2010**, *49*, 561–571 **561**
DOI: 10.1021/ic901730f

Novel Three-Dimensional Pillared-Layer Ln(III)−Cu(I) Coordination Polymers Featuring Spindle-Shaped Heterometallic Building Units

Qi-Bing Bo,* Guo-Xin Sun, and Dong-Ling Geng

School of Chemistry and Chemical Engineering, University of Jinan, Jinan 250022, China

Received September 2, 2009

The hydrothermal reaction of rare earth oxide, CuO, 2,6-pyridinedicarboxylic acid, and 4,4′-bipyridine in the presence of H_3PO_3 resulted in the formation of a new series of 3d-4f heterometallic coordination polymers $[Ln(pydc)_3Cu_3(bipy)_3 \cdot m(H_2O)]_n$ (Ln = Pr (**1**), Nd (**2**), m = 5; Ln = Sm (**3**), Eu (**4**), Gd (**5**), Tb (**6**), Er (**7**), Yb (**8**), m = 4; pydc = 2,6-pyridinedicarboxylate anion; bipy = 4,4′-bipyridine). Complexes **1**−**8** are isostructural and structurally characterized by elemental analysis, FT-IR spectroscopy, thermogravimetry-differential thermal analysis (TG-DTA), single-crystal X-ray diffraction, X-ray powder diffraction (XRPD), and nitrogen adsorption/desorption techniques. The synthesis results show that the addition of H_3PO_3 in the reaction plays an important role in the formation of the compounds. Single-crystal X-ray diffraction analysis reveals that the heterometallic ions are first interconnected by mixing bridging ligands to produce a spindle-shaped heterometallic ring $[Ln_6(pydc)_6Cu_{12}(bipy)_6]$, which is used as the second building unit (SBUs) and finally pillared by bridging bipy molecules to form the rare 3D pillared-layer porous Ln(III)−Cu(I) coordination polymers. Luminescence measurements made under excitation by UV rays reveal that Sm−Cu, Eu−Cu, and Tb−Cu compounds exhibit the characteristic emission bands of Sm^{3+}, Eu^{3+}, and Tb^{3+} ions in the visible regions, respectively; near-infrared (NIR) emission bands from Nd(III) and Yb(III) ions can also be obtained in Nd−Cu and Yb−Cu compounds, respectively; while Pr−Cu, Gd−Cu, and Er−Cu compounds all display similar emission spectra of Cu(I) coordination compounds in the visible regions.

Introduction

The rational design and synthesis of lanthanide-transition metal (d-f) heterometallic coordination polymers are currently attracting a great deal of interests because of their new structural topologies and potential applications as important functional materials in magnetism,[1] luminescent (or luminescent probe) materials,[2] molecular adsorption,[3] and semiconductors.[4] Considering the fact that N and O atoms have affinities to transition-metal and lanthanide ions, respectively, a typical approach toward the construction of d-f heterometallic frameworks can be the reaction of a mixture of d-f heterometallic ions with a single multidentate bridging ligand containing both N- and O-donor atoms. Additionally, to construct new d-f complexes with various structural types, the second auxiliary ligands containing either N- or O-donor atoms are occasionally introduced to the reaction system and further behave as a proper bridge between d and f metal ions.

Up to now, a number of d-f heterometallic complexes have been successfully synthesized through this general strategy.[5] However, to the best of our knowledge, reports on the d^{10}-f^n heterometallic coordination polymers and their luminescent properties are still rare,[6] and most of the reported d^{10}-f^n heterometallic coordination polymers contain

*To whom correspondence should be addressed. E-mail: chm_boqb@ujn.edu.cn.

(1) (a) He, F.; Tong, M.-L.; Yu, X.-L.; Chen, X.-M. *Inorg. Chem.* **2005**, *44*, 559. (b) Zhao, B.; Cheng, P.; Dai, Y.; Cheng, C.; Liao, D. Z.; Yan, S.-P.; Jiang, Z.-H.; Wang, G. L. *Angew. Chem., Int. Ed.* **2003**, *42*, 934. (c) Cheng, J.-W.; Zhang, J.; Zheng, S.-T.; Zhang, M.-B.; Yang, G.-Y. *Angew. Chem., Int. Ed.* **2006**, *45*, 73. (d) Gheorghe, R.; Cucos, P.; Andruh, M.; Costes, J.-P; Donnadieu, B.; Shova, S. *Chem.—Eur. J.* **2006**, *12*, 187. (e) Yue, Q.; Yang, J.; Li, G.-H.; Li, G.-D.; Xu, W.; Chen, J.-S.; Wang, S.-N. *Inorg. Chem.* **2005**, *44*, 5241. (f) Shi, W.; Chen, X.-Y.; Zhao, B.; Yu, A.; Song, H.-B.; Cheng, P.; Wang, H.-G.; Yan, S.-P. *Inorg. Chem.* **2006**, *45*, 3949. (g) Chelebaeva, E.; Larionova, J.; Guari, Y.; Sá Ferreira, R. A.; Carlos, L. D.; Paz, F. A. A.; Trifonov, A.; Guérin, C. *Inorg. Chem.* **2008**, *47*, 775. (h) Wang, N.; Yue, S.; Liu, Y.; Yang, H.; Wu, H. *Cryst. Growth Des.* **2009**, *9*, 368. (i) Hu, X.; Zeng, Y.-F.; Chen, Z.; Sañudo, E. C.; Liu, F.-C.; Ribas, J.; Bu, X.-H. *Cryst. Growth Des.* **2009**, *9*, 421. (j) Zhou, X.-H.; Peng, Y.-H.; Du, X.-D.; Wang, C.-F.; Zuo, J.-L.; You, X.-Z. *Cryst. Growth Des.* **2009**, *9*, 1028. (k) Ren, P.; Shi, W.; Cheng, P. *Cryst. Growth Des.* **2008**, *8*, 1097.

(2) (a) Ronson, T. K.; Lazarides, T.; Adams, H.; Pope, S. J. A.; Sykes, D.; Faulkner, S.; Coles, S. J.; Ward, M. D. *Chem.—Eur. J.* **2006**, *12*, 9299. (b) Chelebaeva, E.; Larionova, J.; Guari, Y.; Ferreira, R. A. S.; Carlos, L. D.; Paz, F. A. A.; Trifonov, A.; Guérin, C. *Inorg. Chem.* **2009**, *48*, 5983. (c) Zhao, B.; Chen, X.-Y.; Cheng, P.; Liao, D.-Z.; Yan, S.-P.; Jiang, Z.-H. *J. Am. Chem. Soc.* **2004**, *126*, 15394. (d) Ye, J.; Zhang, J.; Ye, L.; Xie, D.; Xu, T.; Li, G.; Ning, G. *Dalton Trans.* **2008**, 5342. (e) Zhai, B.; Yi, L.; Wang, H.-S.; Zhao, B.; Cheng, P.; Liao, D.-Z.; Yan, S.-P. *Inorg. Chem.* **2006**, *45*, 8471. (f) Cai, Y.-P.; Zhou, X.-X.; Zhou, Z.-Y.; Zhu, S.-Z.; Thallapally, P. K.; Liu, J. *Inorg. Chem.* **2009**, *48*, 6341. (g) Gao, H.-L.; Zhao, B.; Zhao, X.-Q.; Song, Y.; Cheng, P.; Liao, D.-Z.; Yan, S.-P. *Inorg. Chem.* **2008**, *47*, 11057. (h) Zhao, X.-Q.; Zhao, B.; Shi, W.; Cheng, P. *CrystEngComm* **2009**, *11*, 1261.

(3) (a) Guillou, O.; Daiguebonne, C.; Camara, M.; Kerbellec, N. *Inorg. Chem.* **2006**, *45*, 8468. (b) Wang, Y.; Cheng, P.; Chen, J.; Liao, D.-Z.; Yan, S.-P. *Inorg. Chem.* **2007**, *46*, 4530. (c) Zhao, X.-Q.; Zhao, B.; Ma, Y.; Shi, W.; Cheng, P.; Jiang, Z.-H.; Liao, D.-Z.; Yan, S.-P. *Inorg. Chem.* **2007**, *46*, 5832.

(4) Zhang, J.-J.; Sheng, T.-L.; Hu, S.-M.; Xia, S.-Q.; Leibeling, G.; Meyer, F.; Fu, Z.-Y.; Wu, X.-T. *Chem.—Eur. J.* **2004**, *10*, 3963.

Published on Web 12/17/2009

either coordinated water molecules or OH-groups near the coordination sphere of Ln^{3+}. It is known that the design of the new sensitizing ligands and the d-block transition metal complexes to efficiently sensitize Ln^{3+} emission have been studied extensively in luminescent d-f heterometallic coordination polymers,[7] and the luminescence of Ln^{3+} is often quenched by the nonradiative exchange of electronic energy of Ln^{3+} to the high vibration modes of O−H, N−H, and C−H bonds.[8] In general, coordinated water molecules, and OH- groups are considered to be the most efficient quenchers of Ln^{3+} luminescence.[9] Studies show that each OH-group quenches the excited Ln^{3+} independently, and the quenching efficiency decreases as the distance Ln···OH increases. Therefore, the quenching by the uncoordinated water existing in the crystal is usually smaller than that of coordinated water. It is evident that the luminescence efficiency of lanthanide complexes would be enhanced if the coordinated water molecules were removed from the inner coordination sphere of Ln^{3+}.

In our previous work, we explored a series of functional Ln(III)−Cu(I) coordination polymers formed with mixed bridging ligands in aqueous ethanol,[10] and all the compounds contained the coordinated water molecules. As a result, no intense emission was found in any of them. To construct d^{10}-f^n heterometallic functional coordination polymers with excellent luminescence properties various reaction conditions including the reasonable choice of auxiliary reagent, the mixed metal ions, and the bridging ligands were investigated systematically in our lab. In this paper, a new family of Ln(III)−Cu(I) heterometallic coordination polymers without coordinated water molecules, namely, $[Ln(pydc)_3Cu_3(bipy)_3 \cdot m(H_2O)]_n$ (Ln = Pr (**1**), Nd (**2**), m = 5; Ln = Sm (**3**), Eu (**4**), Gd (**5**), Tb (**6**), Er (**7**), Yb (**8**), m = 4; pydc = 2,6-pyridinedicarboxylate anion; bipy = 4,4′-bipyridine) has been successfully prepared. The syntheses, fascinating structure, robust microporosity, and highly luminescent properties of these compounds will be presented and discussed here.

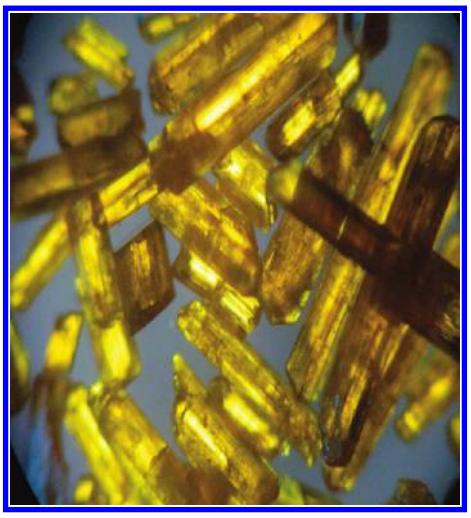

Figure 1. Micrographs of the yellowish prism-shaped crystals enlarged 4×10 times on optical microscope.

Results and Discussion

Description of Crystal Structures. All the compounds are yellowish prism-shaped crystals as shown in Figure 1. Single-crystal X-ray diffraction reveals that complexes **1**−**8** are isostructural and possess a monoclinic crystal system with space group $P2/c$. The crystallographic data and structure refinement details for **1**−**8** are depicted in Table 1.

As shown in Figure 2, lanthanide ions have two types of coordination environments, and all of them chelate to three pydc ligands, showing a coordination number of nine. The subtle distinction between Ln1 and Ln2 originates from three types of the coordination modes of the pdyc ligands: (i) terminal ligand, chelate tridentate to the Ln^{3+} with each carboxyl group attached by one uncoordinated oxygen atom; (ii) μ_3-bridge linking ligand, heptadentate with bis-chelating-bridging mode to Ln1 and different Cu1 atoms; (iii) μ_3-bridge linking ligand, pentadentate with bis-monodentate-bridging mode toward Ln2, Cu2, and Cu3 atoms. To our knowledge, the coordination modes of pdyc ligands in type II are observed for the first time, although pdyc ligands can be used as various bridge-linking ligands to construct coordination polymers.[11]

Figure 3 shows that three kinds of Cu ion coordination environments (Cu1, Cu2, and Cu3) exist in the crystal structures of **1**−**8**, and two different bipy chains bridge the Cu1 and Cu2, Cu3 and Cu3 atoms via the two terminal nitrogen atoms, respectively. Similar to the previously reported three-coordinated Cu(I) complexes,[12] it is evident

(5) (a) Andruh, M.; Costes, J. P.; Diaz, C.; Gao, S. *Inorg. Chem.* **2009**, *48*, 3342. (b) Zhou, Y.; Hong, M.; Wu, X. *Chem. Commun.* **2006**, 135. (c) Ren, Y.-P.; Long, L.-S.; Mao, B.-W.; Yuan, Y.-Z.; Huang, R.-B.; Zheng, L.-S. *Angew. Chem., Int. Ed.* **2003**, *42*, 532. (d) Moushi, E. E.; Stamatatos, T. C.; Wernsdorfer, W.; Nastopoulos, V.; Christou, G.; Tasiopoulos, A. J. *Angew. Chem., Int. Ed.* **2006**, *45*, 7722. (e) Zhang, M.-B.; Zhang, J.; Zheng, S.-T.; Yang, G.-Y. *Angew. Chem., Int. Ed.* **2005**, *44*, 1385. (f) Hoffart, D. J.; Loeb, S. J. *Angew. Chem., Int. Ed.* **2005**, *44*, 901. (g) Luo, F.; Batten, S. R.; Che, Y.; Zheng, J.-M. *Chem.—Eur. J.* **2007**, *13*, 4948. (h) Kou, H.-Z.; Zhou, B. C.; Wang, R.-J. *Inorg. Chem.* **2003**, *42*, 7658. (i) Hong, M. *Cryst. Growth Des.* **2007**, *7*, 10. (j) Cahill, C. L.; Lill, D. T. De; Frisch, M. *CrystEngComm* **2007**, *9*, 15. (k) Cheng, J.-W.; Zheng, S.-T.; Liu, W.; Yang, G.-Y. *CrystEngComm* **2008**, *10*, 1047.

(6) (a) Cheng, J.-W.; Zheng, S.-T.; Ma, E.; Yang, G.-Y. *Inorg. Chem.* **2007**, *46*, 10534. (b) Wang, F.-Q.; Zheng, X.-J.; Wan, Y.-H.; Sun, C.-Y.; Wang, Z.-M.; Wang, K.-Z.; Jin, L.-P. *Inorg. Chem.* **2007**, *46*, 2956. (c) Gu, X.; Xue, D. *Inorg. Chem.* **2007**, *46*, 5349. (d) Gu, X.; Xue, D. *Cryst. Growth Des.* **2006**, *6*, 2551. (e) Gu, X.; Xue, D. *Cryst. Growth Des.* **2007**, *7*, 1726. (f) Gu, X.; Xue, D. *CrystEngComm* **2007**, *9*, 471.

(7) (a) Faulkner, S.; Natrajan, L. S.; Perry, W. S.; Sykes, D. *Dalton Trans.* **2009**, 3890. (b) Moore, E. G.; Samuel, A. P. S.; Raymond, K. N. *Acc. Chem. Res.* **2009**, *42*, 542. (c) Ward, M. D. *Coord. Chem. Rev.* **2007**, *251*, 1663.

(8) (a) Horrocks, W., Jr.; De, W.; Sudnick, D. R. *Acc. Chem. Res.* **1981**, *14*, 384. (b) Richardson, F. S. *Chem. Rev.* **1982**, *82*, 541. (c) Alpha, B.; Ballardini, R.; Balzani, V.; Lehn, J. M.; Perathoner, S.; Sabbatini, N. *Photochem. Photobiol.* **1990**, *52*, 299. (d) Ermolaev, V. L.; Sveshnikova, E. B. *Russ. Chem. Rev.* **1994**, *63*, 905. (e) Kimura, T.; Kato, Y.; Takeishi, H.; Choppin, G. R. *J. Alloy. Compd.* **1998**, *719*, 271. (f) Beeby, A.; Clarkson, I. M.; Dickins, R. S.; Faulkner, S.; Parker, D.; Royle, L.; de Sousa, A. S.; Williams, J. A. G.; Woods, M. J. C. S. *Perkin Trans.* **1999**, *2*, 493.

(9) (a) Parker, D.; Williams, J. A. G. *J. Chem. Soc., Dalton Trans.* **1996**, 3613. (b) Yanagida, S.; Hasegawa, Y.; Murakoshi, K.; Wada, Y.; Nakashima, N.; Yamanaka, T. *Coord. Chem. Rev.* **1998**, *171*, 461. (c) Choppin, G. R.; Peterman, D. R. *Coord. Chem. Rev.* **1998**, *174*, 283. (d) Horrocks, W. DeW., Jr.; Sudnick, D. R. *J. Am. Chem. Soc.* **1979**, *101*, 334. (e) DeSa, G. F.; Malta, O. L.; Donega, C. D.; Simas, A. M.; Longo, R. L.; Santa-Cruz, P. A.; DaSilva, E. F., Jr. *Coord. Chem. Rev.* **2000**, *196*, 165. (f) Werts, M. H. V.; Duin, M. A.; Hofstraat, J. W.; Verhoeven, J. W. *Chem. Commun.* **1999**, 799. (g) Villata, L. S.; Wolcan, E.; Feliz, M. R.; Capparelli, A. L. *J. Phys. Chem. A.* **1999**, *103*, 5661. (h) Li, H. H.; Inoue, S.; Machida, K.; Adachi, G. *Chem. Mater.* **1999**, *11*, 3171.

(10) Bo, Q.-B.; Sun, Z.-X.; Forsling, W. *CrystEngComm* **2008**, *10*, 232.

(11) Huang, Y.-G.; Yuan, D.-Q.; Gong, Y.-Q.; Jiang, F.-L.; Hong, M.-C. *J. Mol. Struct.* **2008**, *872*, 99.

(12) (a) Shimazaki, Y.; Yokoyama, H.; Yamauchi, O. *Angew. Chem., Int. Ed.* **1999**, *38*, 2401. (b) Lo, S. M.-F.; Chui, S. S.-Y.; Shek, L.-Y.; Lin, Z.; Zhang, X. X.; Wen, G.- H.; Williams, I. D. *J. Am. Chem. Soc.* **2000**, *122*, 6293. (c) Zhang, X.-M.; Tong, M.-L.; Chen, X.-M. *Angew. Chem., Int. Ed.* **2002**, *41*, 1029. (d) Sha, J.; Peng, J.; Liu, H.; Chen, J.; Dong, B.; Tian, A.; Su, Z. *Eur. J. Inorg. Chem.* **2007**, *9*, 1268. (e) Zheng, L.-M.; Yin, P.; Xin, X.-Q. *Inorg. Chem.* **2002**, *41*, 4084.

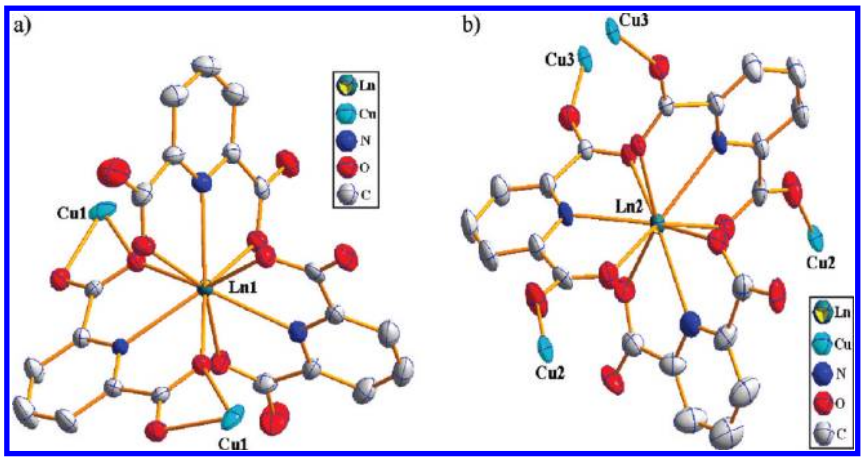

Figure 2. (a) ORTEP diagram showing the coordination environment of Ln1cations. (b) An ORTEP diagram showing the coordination environment of Ln2 cations (hydrogen atoms, bipy, and water molecules are omitted for clarity).

Table 1. Crystallographic Data and Structure Refinement Details for **1**−**8**

compound	**1**	**2**	**3**	**4**
empirical formula	$C_{51}H_{43}O_{17}N_9Cu_3Pr$	$C_{51}H_{43}O_{17}N_9Cu_3Nd$	$C_{51}H_{41}O_{16}N_9Cu_3Sm$	$C_{51}H_{41}O_{16}N_9Cu_3Eu$
formula weight	1385.48	1388.82	1376.92	1378.52
crystal system	monoclinic	monoclinic	monoclinic	monoclinic
space group	*P*2/*c*	*P*2/*c*	*P*2/*c*	*P*2/*c*
a/Å	23.738(2)	23.680(2)	23.657(2)	23.682(5)
b/Å	10.598(12)	10.5601(12)	10.515(11)	10.546(2)
c/Å	21.660(2)	21.642(2)	21.695(2)	21.648(4)
α/deg	90	90	90	90
β/deg	105.239(2)	105.406(2)	105.124(10)	105.280(3)
γ/deg	90	90	90	90
volume/ Å^3	5257.2(8)	5217.4(8)	5209.7(9)	5215.4(18)
Z	4	4	4	4
ρ_{cal} /g·cm^{-3}	1.750	1.768	1.756	1.756
μ /mm^{-1}	2.190	2.268	2.399	2.473
F (000)	2776	2780	2748	2752
GOF	1.056	1.032	1.104	1.002
final *R* indices	*R*1 = 0.0331	*R*1 = 0.0426	*R*1 = 0.0976	*R*1 = 0.0282
[*I* > 2*σ*(*I*)]	*wR*2 = 0.0774	*wR*2 = 0.0955	*wR*2 = 0.2166	*wR*2 = 0.0685
R indices	*R*1 = 0.0473	*R*1 = 0.0743	*R*1 = 0.1201	*R*1 = 0.0359
all data	*wR*2 = 0.0845	*wR*2 = 0.1131	*wR*2 = 0.2259	*wR*2 = 0.0718

compound	**5**	**6**	**7**	**8**
empirical formula	$C_{51}H_{41}O_{16}N_9Cu_3Gd$	$C_{51}H_{41}O_{16}N_9Cu_3Tb$	$C_{51}H_{41}O_{16}N_9Cu_3Er$	$C_{51}H_{41}O_{16}N_9Cu_3Yb$
formula weight	1383.81	1385.48	1393.82	1399.60
crystal system	monoclinic	monoclinic	monoclinic	monoclinic
space group	*P*2/*c*	*P*2/*c*	*P*2/*c*	*P*2/*c*
a/Å	23.550(5)	23.660(3)	23.593(2)	23.586(2)
b/Å	10.400(2)	10.513(11)	10.4448(12)	10.4497(10)
c/Å	21.530(4)	21.702(2)	21.641(2)	21.655(2)
α/deg	90	90	90	90
β/deg	105.030(3)	105.241(2)	105.175(2)	105.252(2)
γ/deg	90	90	90	90
volume/ Å^3	5092.7(18)	5208.3(10)	5146.9(9)	5149.2(9)
Z	4	4	4	4
ρ_{cal} /g·cm^{-3}	1.805	1.767	1.799	1.805
μ /mm^{-1}	2.604	2.630	2.918	3.103
F (000)	2756	2760	2772	2780
GOF	1.006	1.145	1.292	1.046
final *R* indices	*R*1 = 0.0427	*R*1 = 0.0627	*R*1 = 0.0975	*R*1 = 0.0321
[*I* > 2*σ*(*I*)]	*wR*2 = 0.1316	*wR*2 = 0.1311	*wR*2 = 0.3558	*wR*2 = 0.0689
R indices	*R*1 = 0.0508	*R*1 = 0.0768	*R*1 = 0.1151	*R*1 = 0.0482
all data	*wR*2 = 0.1376	*wR*2 = 0.1360	*wR*2 = 0.3709	*wR*2 = 0.0754

that both Cu2 and Cu3 ions are three-coordinated by one carboxylate oxygen atom from the same pydc ligand and the two nitrogen atoms from two different bipy ligands, and have a "T-shape" geometry. Unlike the Cu2 and Cu3 ions, the tetrahedral coordination geometry of a Cu1 ion is formed by two carboxyl O atoms from one pydc ligand and two nitrogen atoms from two bipy ligands (Figure S1 in Supporting Information). To our knowledge, this type of coordination mode of Cu^+ in pydc complex is uncommon and is observed for the first time.

Furthermore, as depicted in Table 2, the shortest separation lengths for Ln···Ln, Ln···Cu, and Cu···Cu are 10.8415, 5.0047, and 3.4355 Å, respectively. The distances of Ln1−O, Ln1−N, Ln2−O, Ln2−N, Cu1−O, Cu1−N, Cu2−O, Cu2−N, Cu3−O, and Cu3−N for all the compounds fall in the range of 2.3619(3)−2.5173(3), 2.4445(2)−2.5943(3), 2.3575(3)−2.5196(3), 2.4264(5)−2.6137(3), 2.2113(4)−2.7392(1), 1.8970(5)−1.9380(1), 2.2308(4)−2.2682(4), 1.8806(1)−1.9401(1), 2.2505(5)−2.2954(3), and 1.8943(2)−1.9210(3) Å, respectively. The average Ln−O and Ln−N bond lengths of the compounds **1**−**8** gradually decrease with the series of lanthanides except for compound **5** (Figure 4), because of the presence of significant lanthanide contraction and gadolinium break effect in the series of isomorphous compounds.

Because of the synergistic coordination between heterometallic ions (two Ln ions and three Cu ions) and mixed bridge linking ligands (two types of pydc and bipy), the spindle-shaped subunits containing an 18-nuclear Ln_6Cu_{12} ring are formed running along the *c*- axis (Figure 5). It is noticeable that the spindle-shaped heterometallomacrocycle has a puckered structure (Figure S2 in Supporting Information), and the lanthanide pseudohexagon lies in a chair form like a cyclohexyl ring (Figure S3 and Figure S4 in Supporting Information). It is evident that three planes (plane 1, 2, and 3) consisting of six different Ln(III) ions are generated in one spindle-shaped subunit, two of them (plane 1 and 3) are parallel and project above and below the third one (plane 2). The dihedral angle between "plane 1" and "plane 2" is averaged to be 34.7754°, and the estimated distance between

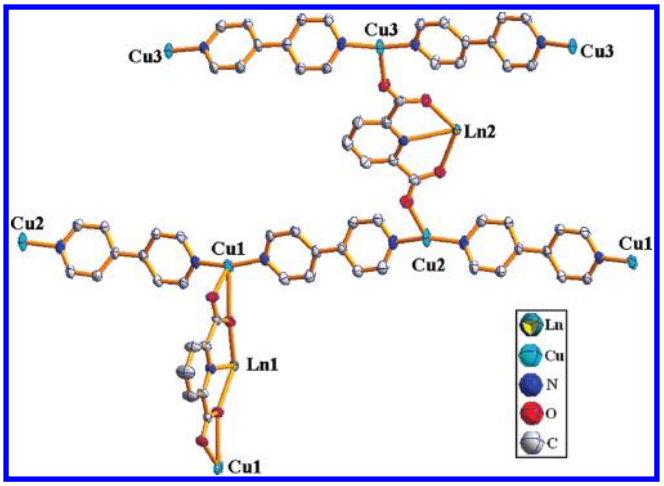

Figure 3. Cu ion coordination environments.

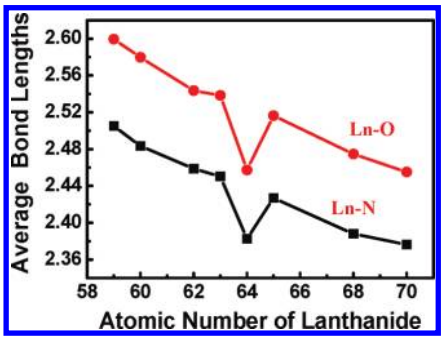

Figure 4. Lanthanide contraction and gadolinium break effect in compounds **1**−**8**.

Table 2. Selected Bonds and the Shortest Separation Lengths (Å) for **1**−**8**

	1	**2**	**3**	**4**	**5**	**6**	**7**	**8**
Ln1−O_{pydc}	2.5149(3)	2.4981(4)	2.4756(1)	2.4570(2)	2.3685(4)	2.4365(5)	2.4090(1)	2.3619(3)
	2.5149(3)	2.4981(4)	2.4756(1)	2.4570(2)	2.3685(4)	2.4365(5)	2.4090(1)	2.3619(3)
	2.4820(3)	2.4955(4)	2.4363(9)	2.4321(2)	2.3837(4)	2.4430(6)	2.3767(1)	2.3800(3)
	2.4820(3)	2.4955(4)	2.4363(9)	2.4321(2)	2.3837(4)	2.4430(6)	2.3767(1)	2.3800(3)
	2.5173(3)	2.4592(4)	2.4627(9)	2.4615(2)	2.3893(4)	2.4002(6)	2.3944(1)	2.3893(3)
	2.5172(3)	2.4592(4)	2.4627(9)	2.4615(2)	2.3893(4)	2.4002(6)	2.3944(1)	2.3893(3)
Ln1−N_{pydc}	2.5928(4)	2.5723(6)	2.5279(1)	2.5363(3)	2.4478(5)	2.5047(8)	2.4681(1)	2.4541(4)
	2.5943(3)	2.5741(5)	2.5279(1)	2.5363(3)	2.4478(5)	2.5047(8)	2.4681(1)	2.4541(4)
	2.5943(3)	2.5741(5)	2.5288(1)	2.5355(3)	2.4593(7)	2.5072(9)	2.4445(2)	2.4483(4)
Ln2−O_{pydc}	2.5073(3)	2.4615(4)	2.4454(8)	2.4656(3)	2.4032(5)	2.4264(6)	2.4026(1)	2.3575(3)
	2.5073(3)	2.4615(4)	2.4454(8)	2.4656(3)	2.4032(5)	2.4264(6)	2.4026(1)	2.3575(3)
	2.4892(3)	2.5037(5)	2.4554(9)	2.4302(2)	2.3689(4)	2.4438(8)	2.3763(1)	2.3983(3)
	2.4892(3)	2.5037(5)	2.4554(9)	2.4302(2)	2.3689(4)	2.4438(8)	2.3763(1)	2.3983(3)
	2.5196(3)	2.4827(4)	2.4776(1)	2.4554(2)	2.3818(4)	2.4114(6)	2.3688(1)	2.3713(3)
	2.5196(3)	2.4827(4)	2.4776(1)	2.4554(2)	2.3818(4)	2.4114(6)	2.3688(1)	2.3713(3)
Ln2−N_{pydc}	2.6137(3)	2.5997(5)	2.5749(1)	2.5523(3)	2.4786(5)	2.5421(7)	2.5039(1)	2.4739(4)
	2.6137(3)	2.5997(5)	2.5749(1)	2.5523(3)	2.4786(5)	2.5421(7)	2.5039(1)	2.4739(4)
	2.5873(5)	2.5586(7)	2.5265(2)	2.5175(4)	2.4316(7)	2.4968(1)	2.4590(2)	2.4264(5)
Cu1−O_{pydc}	2.6587(3)	2.2577(4)	2.2488(9)	2.2442(2)	2.7348(4)	2.2330(6)	2.2180(1)	2.7347(3)
	2.2601(3)	2.6589(4)	2.6928(9)	2.6901(2)	2.2113(4)	2.7096(5)	2.7392(1)	2.2145(3)
Cu1−N_{bpy}	1.9215(3)	1.9182(4)	1.9209(1)	1.9041(3)	1.8970(5)	1.9220(7)	1.9303(1)	1.9224(4)
	1.9265(3)	1.9248(5)	1.9380(1)	1.9148(3)	1.9118(5)	1.9281(7)	1.9242(1)	1.9210(4)
Cu2−O_{pydc}	2.2682(4)	2.2525(5)	2.2665(1)	2.2496(3)	2.2344(5)	2.2517(7)	2.2351(1)	2.2308(4)
Cu2−N_{bpy}	1.9283(4)	1.9214(5)	1.9401(1)	1.9196(3)	1.9170(5)	1.9329(7)	1.9284(1)	1.9286(4)
	1.9157(3)	1.9188(4)	1.8873(1)	1.9313(3)	1.9041(4)	1.9055(7)	1.8806(1)	1.9123(3)
Cu3−O_{pydc}	2.2954(3)	2.2803(4)	2.2713(1)	2.2776(3)	2.2505(5)	2.2657(7)	2.2513(1)	2.2560(3)
Cu3−N_{bpy}	1.9041(3)	1.9073(5)	1.8825(1)	1.9210(3)	1.9138(5)	1.9103(7)	1.9010(2)	1.9063(4)
	1.9126(3)	1.8998(5)	1.9147(1)	1.9200(3)	1.9080(5)	1.9013(7)	1.8943(2)	1.9078(4)
Ln···Ln	10.8434(1)	10.8378(1)	10.8614(1)	10.8426(2)	10.7852(2)	10.8686(1)	10.8430(1)	10.8502(1)
Ln···Cu	5.0099(6)	4.9973(1)	5.0054(2)	5.0078(1)	5.0001(2)	5.0085(1)	5.0055(2)	5.0030(8)
Cu···Cu	3.4632(9)	3.4509(1)	3.4414(3)	3.4482(9)	3.4022(1)	3.4404(2)	3.4185(3)	3.4189(9)

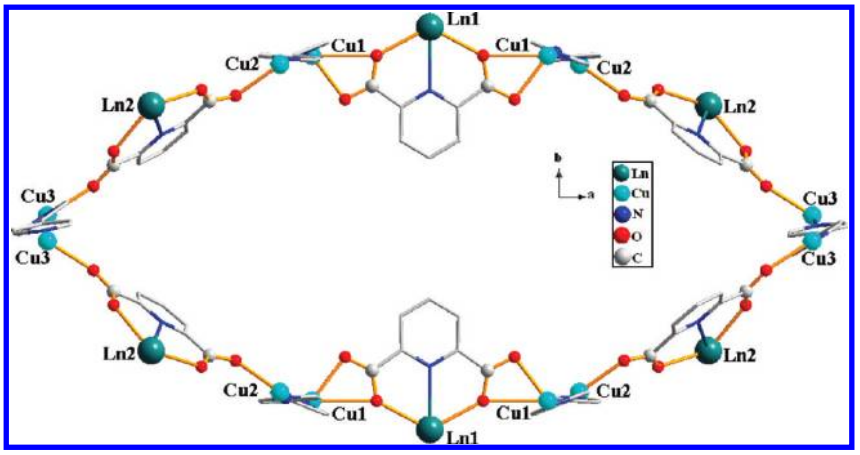

Figure 5. Perspective view of the spindle-shaped ring based on pydc and bipy-bridged Ln_6Cu_{12} heterometallic units (terminal pydc ligands are omitted for clarity).

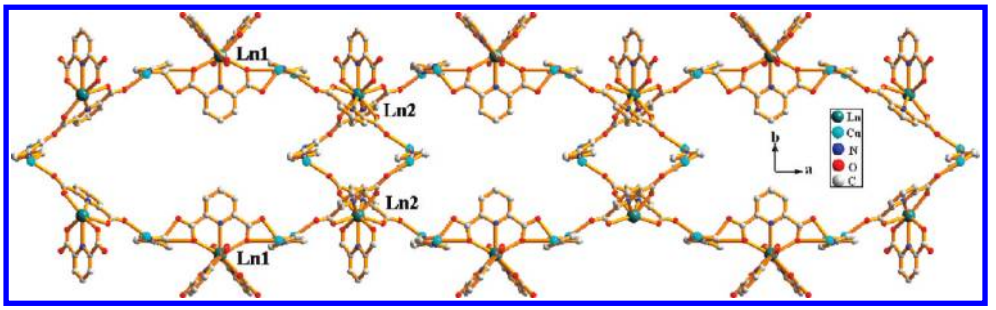

Figure 6. View of the 1D chain self-penetrated by three adjacent spindle-shaped rings (hydrogen atoms and lattice water molecules are omitted for clarity).

"plane 1" and "plane 3" is about 11.1424 Å. Furthermore, the distances of Ln−Ln in the planes fall in the range of 35.7927(9)−36.0963(2), 14.5176(2)−14.7804(8), and 18.1707(4)−18.3338(1) Å for *a*, *b*, and *c*, separately (Table S1 in Supporting Information).

The remarkable structure feature of the spindle-shaped ring is that the void in it is large enough to include other ligands because nature dislikes vacuums. As a result, each of the spindle-shaped rings used as SBUs is further self-penetrated via two metal knots (Ln2) to form a neutral one-dimensional (1D) coordination polymer chain with the composition $[Ln_6(pydc)_6Cu_{12}(bipy)_6]_n$ along the *a*-axis (Figure 6). Because of the presence of the extensive hydrogen-bonding interactions between the carboxylate oxygen atoms of pydc ligands and free water molecules in the lattice, the adjacent polymeric 1D chains are packed in parallel into the layered two-dimensional (2D) networks along the *ab* plane as shown in Figure 7. The hydrogen bonds for the representative compounds $[Pr(pydc)_3Cu_3(bipy)_3\cdot 5(H_2O)]_n$ and $[Tb(pydc)_3Cu_3(bipy)_3\cdot 4(H_2O)]_n$ show that the O···O distances range from 2.738 Å to 3.197 Å, and the O−H···O angles from 125.63° to 179.83°, respectively (Table S2 in Supporting Information). At the same time, these adjacent layers are pillared together by neutral bipyridine ligands, finally leading to the formation of an infinite 3D pillared-layer porous framework.

Here, six pillared bipy molecules can be clearly seen between the layers as shown in Figure 8. The Cu···Cu distance linked by one bipy molecule in adjacent layers is estimated to be about 10.871 and 10.922 Å for Cu3−Cu3 and Cu1−Cu2, respectively (Table S3 in Supporting Information). The pyridine rings of six bipy molecules deviate significantly from planarity, and the dihedral angle between the mean planes of the two pyridyl rings is also listed (Table S3 in Supporting Information). It can be seen that there are two types of pillars: type I for pillar 1 and 4; type II for pillars 2, 3, 5, and 6. The average dihedral angle of the 4,4′-bipyridine in **1**−**8** is about 22.203° and 26.474° for type I and II pillars, respectively.

It is noteworthy that the regulated arrangement of the pillars and the spindle-shaped heterometallic building units also creates two kinds of the apparent 1D channels with a window shape along the *c*-axis (Figure 9). The size of the window-shape section is estimated to be 9.1309 × 14.6532 $Å^2$ for one channel, and 17.1836 × 19.5329 $Å^2$ for the other dimensions (Table S4 in Supporting Information, calculated from the distance between two closest Cu and Ln ions). The former channels are only occupied by part of the free water molecules, while the latter ones are partially filled with bridge-linking ligands pydc and the free water molecules. Furthermore, the 3D porous network is stable after removal of all the free water molecules, as indicated by thermogravimetry-differential thermal analysis (TG-DTA) and PXRD measurements described below.

Metal Ions Oxidation State Analysis. The program, Bond Valence Calculator,[13] kindly provided by Prof. I. D. Brown, is designed to calculate bond valences from the bond lengths. The bond valence sum calculations (BVS) show that all the lanthanide and Cu metal centers in compounds **1**−**8** are in the +3 and +1 oxidation state,

(13) (a) Brown, I. D. *Acta Crystallogr.* **1977**, *B33*, 1305. (b) *Bond Valence Calculator*, Ver.2.0; 1993.

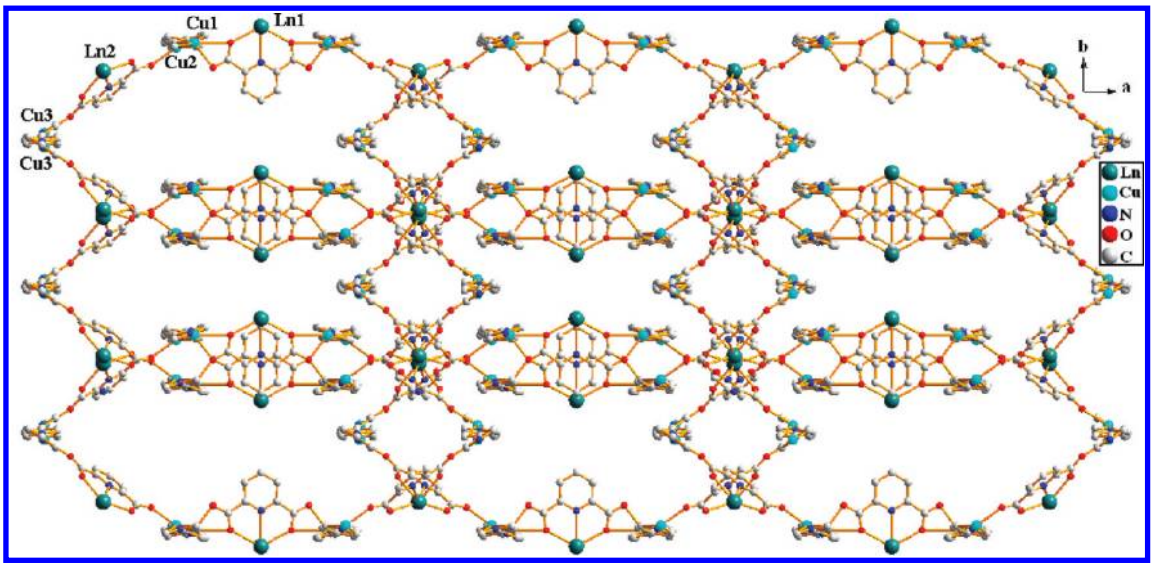

Figure 7. View of the parallelly packing structure of three 1D chains showing 2D Layers constructed by hydrogen bonding along *c* axis (terminal pydc ligands, hydrogen atoms and water molecules are omitted for clarity).

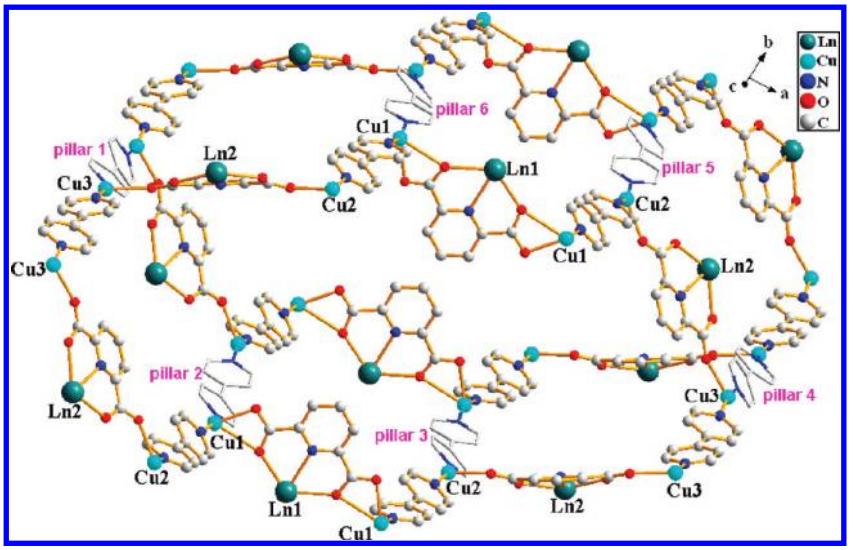

Figure 8. View of the pillared layer structure slightly offset from the *c* axis, showing six pillared bipy molecules (wire-stick representation) incorporated regularly between the two sheets.

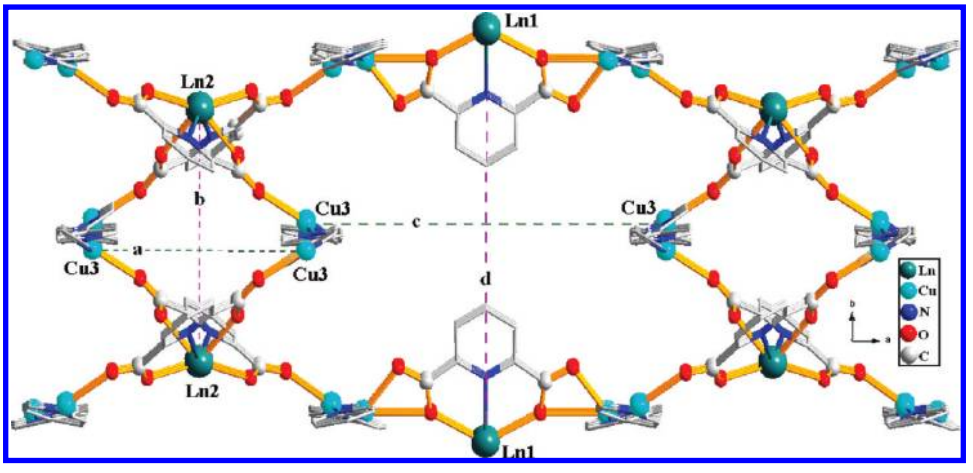

Figure 9. 1D channels with the window shape along the *c*-axis (pyridine rings are represented as wire-stick and hydrogen atoms and water molecules are omitted for clarity).

respectively (Table S5−S13 in the Supporting Information).

It should be pointed out that although CuO is used as the starting reactant, the oxidation state of copper atoms is +1 in the final products. It appears that the reaction chemistry is quite interesting, and the formation of the samples is strongly influenced by the reaction conditions. To clarify the complexity of the present reaction, we also performed the contrast experiments without H_3PO_3. The results showed that only unspecific precipitates or sky-blue solution were obtained in the reaction vessel. Considering the fact that the Cu(II) complex is usually a green or blue color, while the Cu(I) complex often exhibits a red or pale yellow color, it is easily understandable that the H_3PO_3 molecule plays a key role in the formation of Cu(I) complex crystals. Furthermore, studies about H_3PO_3 used as a reductant have been reported extensively.[14] Therefore, the reductive effect of the H_3PO_3 on the process of $Cu^{2+} \rightarrow Cu^{+}$ is more distinct in the present reaction, although some similar reduction processes have been proposed to be related to the bipy or pyridine derivatives under solvothermal conditions.[15] The results of metal ions oxidation state analysis, combined with elemental analysis below, further confirmed the rationality of the composition of compounds **1**−**8**.

FT-IR Spectra Analysis. Since complexes **1**−**8** have the same mixed ligands and Ln(III)−Cu(I) centers, only the FT-IR results of the complex **2** are shown as the example (Figure S5−S6 in Supporting Information). A broadband centered around 3422 cm^{-1} is assigned to the O−H stretching frequency of the lattice water molecules. The absence of the characteristic bands of the protonated carboxylic group at about 1700 cm^{-1} indicates the complete deprotonation of 2,6-pyridinedicarboxylic acid ligand upon reaction with metal ions. On the other hand, the IR spectrum of the complex **2** clearly shows that the characteristic bands of the 2,6-pyridinedicarboxy late groups are split into dual peaks: 1619 cm^{-1} and 1573 cm^{-1} for the asymmetric stretching and 1431 cm^{-1}, 1384 cm^{-1} for symmetric stretching. This indicates that the 2,6-pyridinedicarboxylate groups adopt different coordination fashions in the complex.[16] The peaks at 1619 cm^{-1} and 1384 cm^{-1} are assigned to the υ_{as} (asymmetric vibration) and υ_s (symmetric vibration) of the singly coordinated carboxyl group, while the peaks at 1573 cm^{-1} and 1431 cm^{-1} are attributed to the υ_{as} and υ_s of the bridging carboxyl group. The $\Delta\upsilon$ between υ_{as}-(COO^-) and υ_s (COO^-) are at 235 and 142 cm^{-1}, respectively, which are in accordance with the established rule[16] and the result of the single-crystal X-ray analysis. In addition, the characteristic bands at 1485, 1217, 1188, 1071, 1022, and 916 cm^{-1} perhaps are related to the pyridine rings of the bipy molecules, and the characteristic bands at 813, 772, 728, 697, 661, and 492 cm^{-1} can be regarded as the vibration frequencies of Ln−O and Cu−O bonds.[16]

(14) (a) Moondra, A.; Mathur, A.; Banerji, K. K. *J. Chem. Soc., Dalton Trans.* **1990**, *9*, 2697. (b) Bshnoi, G.; Sharma, M.; Sindal, R. S.; Sharma, P. K. *J. Indian Chem. Soc.* **2007**, *84*, 892.

(15) (a) Zhang, X.-M. *Coord. Chem. Rev.* **2005**, *249*, 1201. (b) Chen, X.-M.; Tong, M.-L. *Acc. Chem. Res.* **2007**, *40*, 162.

(16) Nakamoto, K. *Infrared and Raman Spectra of Inorganic and Coordination Compounds*; John Wiley & Sons: New York, 1986.

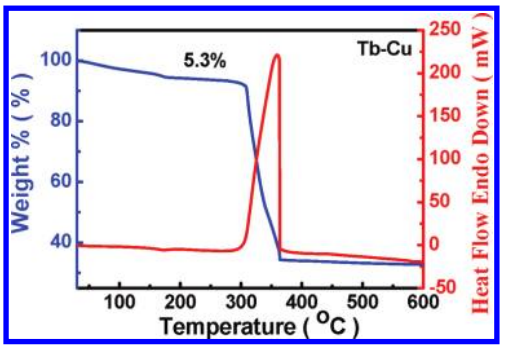

Figure 10. TG-DTA of compound **6**.

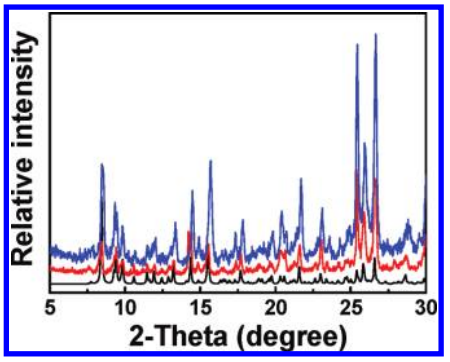

Figure 11. XRPD patterns of the simulated (bottom), as-synthesized (middle), and dried compound **6** (top) (as a representative example).

TG-DTA Analyses and X-ray Powder Diffraction (XRPD). To investigate the thermal stabilities of the compounds and illustrate whether the 3D pillared-layer porous framework is robust, TG-DTA and XRPD analyses were performed. Because of the similarity of the thermal decomposition behaviors in **1**−**8**, a representative example of **6** is discussed here. As shown in Figure 10, the TGA curves of **6** display two distinct weight losses. The first one from room temperature to 160 °C with an inconspicuous endothermic peak corresponds to the loss of the lattice water molecule. The observed weight loss of 5.3% is in close agreement with the calculated value of 5.2%. The second weight loss of 64.2% with a distinctly exothermic peak corresponds to the burning of the organic groups from 290 to 370 °C, which is slightly lower than the corresponding theoretical value of 68.3%. The final residuals are mixed metal oxides. It should be noted that no weight loss is observed in the temperature range 160−280 °C, which means that the formed framework formulated as $[Tb(pydc)_3Cu_3(bipy)_3]$ is robust and stable below 280 °C, and collapses beyond this temperature. This excellent thermal stability is further confirmed by the following XRPD patterns of the sample **6** dried under high vacuum at 180 °C.

As shown in Figure 11, the XRPD patterns for the sample dried under high vacuum at 180 °C and the as-synthesized sample of **6** are similar to each other, and are all in close agreement with the XRPD patterns simulated from the respective single-crystal X-ray data using the Mercury 1.4 program, although the intensities of some peaks show some differences because of the preferred orientation of the powder samples. Furthermore, the TG-DTA results of the dried sample also show that the free water molecules indeed disappear (Figure 12).

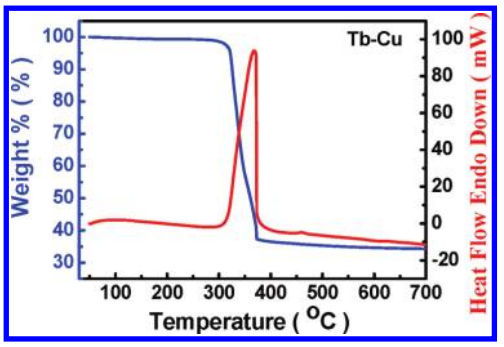

Figure 12. TG-DTA of compound **6**, dried under high vacuum at 180 °C.

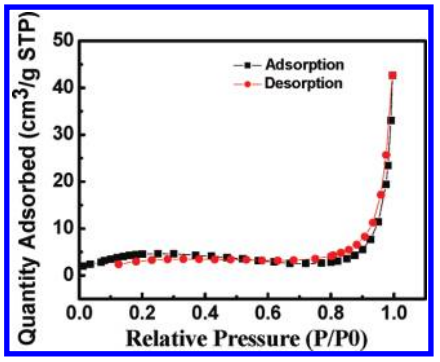

Figure 13. Nitrogen adsorption and desorption isotherms of Tb−Cu at 77 K, showing microporous adsorption and desorption for Nitrogen.

These results confirm that the single-crystal structures are really representative of the bulk of the corresponding samples, and that the porous network of **6** is retained after the removal of the lattice water molecules.

N_2 Adsorption−Desorption Measurements. Because all the compounds are isostructural, sample **6** is selected as a representative example to measure the nitrogen adsorption and desorption isotherms at 77 K to evaluate its microporous property, and the results are shown in Figure 13. Herein, a known weight (142.1 mg) of the as-synthesized sample is first placed in the quartz tube, and the sample is dried under high vacuum at 180 °C for 24 h to remove the solvated water molecules before subsequent measurement. The results of TG/DTA (Figure 12) and XRPD (Figure 11) confirm that all the free water molecules in the dried sample are removed, and the framework remains intact. As shown in Figure 13, it is evident that the adsorption isotherm shows a smooth rise at very low relative pressure and a plateau after saturation, then a very slow stepping-up at 0.77 P/P_0 region, which is characteristics of microporous (type I) adsorbents, and what occurred before 0.77 P/P_0 can be attributed to the process of the nitrogen filling into the micropores.[17] The isotherm goes up steeply after 0.92 P/P_0 and reaches the high-point with the maximum adsorption amount of 42.74 cm^{-3}/g, displaying much nitrogen being absorbed and some mesopore formed by powder interspaces of the dehydrated material. On the other hand, the adsorption curve coincides with the desorption curve at low 0.58 P/P_0, which indicates that the microporous frameworks are very stable.

(17) Kitagawa, S.; Kitaura, R.; Noro, S.-I. *Angew. Chem., Int. Ed.* **2004**, *43*, 2334.

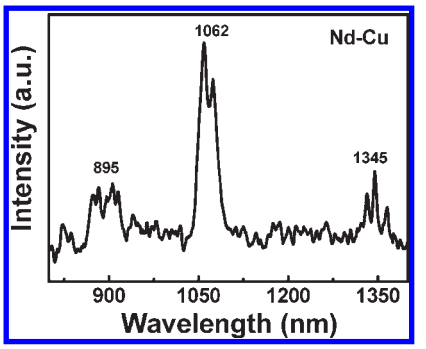

Figure 14. Emission spectra of **2** excited at 280 nm in the solid state at room temperature.

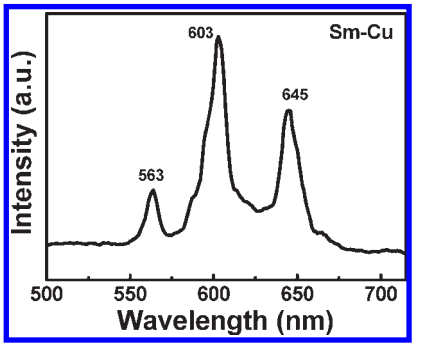

Figure 15. Emission spectra of **3** excited at 275 nm in the solid state at room temperature.

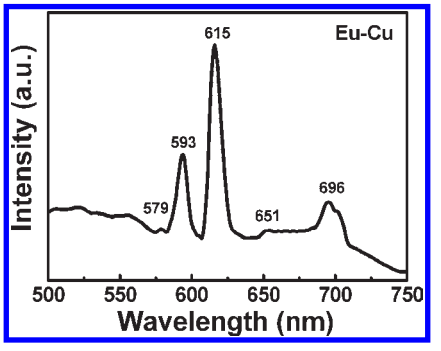

Figure 16. Emission spectra of **4** excited at 275 nm in the solid state at room temperature.

Photoluminescent Properties. Because of the excellent luminescent properties of lanthanide compounds and d^{10} metal complexes, the solid-state luminescence of **1**−**8** was investigated at room temperature (Figure 14−19). The interesting results show that compounds **2**, **3**, **4**, **6**, and **8** display the characteristic emission of Nd^{3+}, Sm^{3+}, Eu^{3+}, Tb^{3+}, and Yb^{3+}, respectively, while **1**, **5**, and **7** all exhibit similar emission spectra of Cu(I) coordination compounds.

As shown in Figure 14, compound **2** displays three sets of emission bands characteristic of the Nd^{3+} ion in the near-IR region with an excitation wavelength of 280 nm: it has the strongest emission band at 1062 nm ($^4F_{3/2}\rightarrow{}^4I_{11/2}$), a broad emission band centered at 895 nm ($^4F_{3/2}\rightarrow{}^4I_{9/2}$) with a much lower intensity, and a sharp weak band at 1345 nm ($^4F_{3/2}\rightarrow{}^4I_{13/2}$), which are consistent with the previously reported spectra of Nd(III) complexes.[18]

(18) (a) Huang, Y.-L.; Huang, M.-Y.; Chan, T.-H.; Chang, B.-C.; Lii, K.-H. *Chem. Mater.* **2007**, *19*, 3232. (b) Zucchi, G.; Maury, O.; Thuéry, P.; Ephritikhine, M. *Inorg. Chem.* **2008**, *47*, 10398.

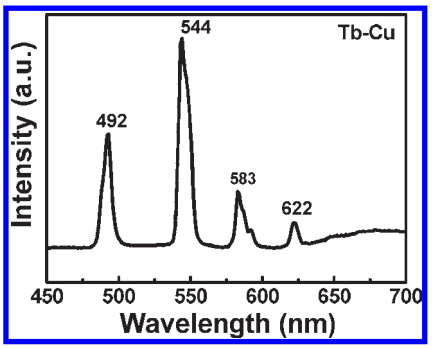

Figure 17. Emission spectra of **6** excited at 275 nm in the solid state at room temperature.

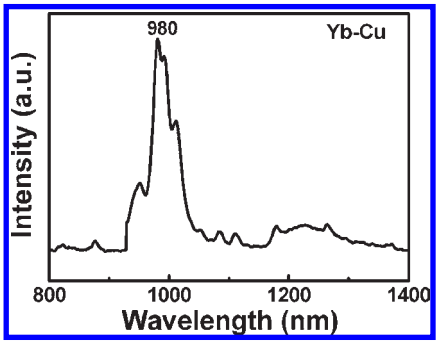

Figure 18. Emission spectra of **8** excited at 275 nm in the solid state at room temperature.

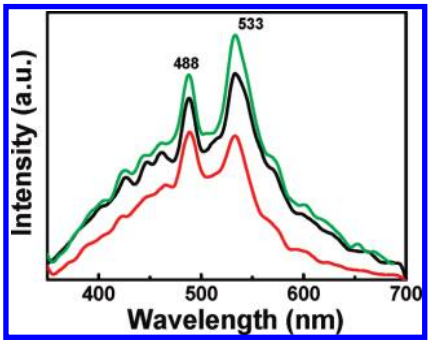

Figure 19. Emission spectra of **1** (bottom), **5** (middle), and **7** (top) excited at 240 nm in the solid state at room temperature.

Complex **3** exhibits intense pink emission when excited at 275 nm (Figure 15). The three characteristic peaks at 563, 603, and 645 nm are attributed to Sm^{3+} transitions from $^4G_{5/2}$ to ^6H_J (J = 5/2, 7/2, 9/2), respectively. The most intense peak is the transition $^4G_{5/2}\rightarrow{}^6H_{7/2}$ at 603 nm.

Compound **4** yields intense red luminescence when measured from 500 to 750 nm upon excitation at 275 nm and exhibits the characteristic transition $^5D_0\rightarrow{}^7F_J$ (J = 0−4) of Eu^{3+} with emission bands 579, 593, 615, 651, and 696 nm, respectively (Figure 16), which may be attributed to the efficient ligand to metal (Eu) energy transfer (LMCT). On the other hand, it is known that the intensity of the $^5D_0\rightarrow{}^7F_2$ transition (electric dipole) to the $^5D_0\rightarrow{}^7F_1$ transition (magnetic dipole) is widely used as a measure of the coordination state and the site symmetry of the europium ion. In complex **4**, it is evident that the red emission of $^5D_0\rightarrow{}^7F_2$ is the most intense and is the preferred transition for Eu-containing luminescent materials. The intensity ratio of $I(^5D_0\rightarrow{}^7F_2)/I(^5D_0\rightarrow{}^7F_1)$ is about 2.42, which indicates that Eu^{3+} is not lying in a centrosymmetric coordination and has lower symmetric coordination environment in **4**. This has been confirmed by the appearance of the symmetry-forbidden emission $^5D_0\rightarrow{}^7F_0$ at 579 nm.[19] All these are consistent with the result of the single-crystal X-ray analysis.

Compound **6** emits the hypersensitive green light under excitation of 275 nm and exhibits the characteristic transition $^5D_4\rightarrow{}^7F_J$ (J = 3−6) of the Tb^{3+} ion: the strongest emission peak at 544 nm ($^5D_4\rightarrow{}^7F_5$) with a shoulder, the second strongest emission peak at 492 nm ($^5D_4\rightarrow{}^7F_6$), two weak emission peaks at 583 nm ($^5D_4\rightarrow{}^7F_4$) and 622 nm ($^5D_4\rightarrow{}^7F_3$) (Figure 17).

Complex **8** displays a strong emission at 980 nm upon excitation of 275 nm (Figure 18), which is the characteristic transition $^2F_{5/2}\rightarrow{}^2F_{7/2}$ of the Yb^{3+} ion in near-infrared region.[20]

The complexes **1**, **5**, and **7** emit very similar and strong photoluminescence of Cu(I) complexes at room temperature in the solid state (Figure 19). According to the emission spectra of other Cu(I) coordination compounds reported,[21] two intense emission peaks observed at 488 and 532 nm under 240 nm UV light photoexcitation can be tentatively assigned to metal-to-ligand charge transfer triplet excited states (^{3}[MLCT]).

From the photo luminescent properties of compounds **1**−**8** mentioned above, it can be seen that, under excitation of UV rays, the emissions of solid samples containing Sm(III)−Cu(I), Eu(III)−Cu(I), and Tb(III)−Cu(I) ions have all been efficiently sensitized by the mixed organic ligands in the visible region at room temperature and exhibit the characteristic transition of the Sm^{3+}, Eu^{3+}, and Tb^{3+} ions, respectively. As for samples containing Nd(III)−Cu(I) and Yb(III)−Cu(I), they also display the characteristic emission bands for the Nd^{3+} and Yb^{3+} ions in the near-IR region. Interestingly, samples containing Pr(III)−Cu(I), Gd(III)−Cu(I), and Er(III)−Cu(I) give typical emission spectrum of Cu(I) coordination compounds. The energy transfer process in lanthanide(III)−copper(I) coordination polymers appears to have selectivity between d^{10}-f^n heterometallic ions and mixed organic ligands. The detailed mechanism of its selectivity needs further study in the future. On the other hand, according to the theory of energy transfer,[22] more efficient energy transfer from ligands to Ln(III) centers in compounds **2**, **3**, **4**, **6**, and **8** than that of the heterometallic coordination polymers $[\{Ln_2(SO_4)_2(H_2O)_2(pydc)_2Cu_2(bipy)_2\cdot 2(H_2O)\}]_n$ [10] should be concluded because of the presence of coordinated water molecules in the latter but not the former case.

(19) Bünzli, J.-C. G; Piguet, C. *Chem. Soc. Rev.* **2005**, *34*, 1048.
(20) (a) Deun, R. V.; Nockemann, P. F.; Hecke, P. V.; Meervelt, K. V.; Binnemans, L. K. *Inorg. Chem.* **2006**, *45*, 10416. (b) Shavaleev, N. M.; Accorsi, G. V. D.; Lazarides, Z. R. B.; Calogero, T. G.; Armaroli, N. W. M. *Inorg. Chem.* **2005**, *44*, 61. (c) Ziessel, R. F.; Ulrich, G.; Charbonnière, L.; Imbert, D.; Scopelliti, R.; Bünzli, J.-C. G. *Chem.—Eur. J.* **2006**, *12*, 5060.
(21) (a) Cambot, A. L.; Cantuel, M.; Leydet, Y.; Jonusauskas, G.; Bassani, D. M.; McClenaghan, N. D. *Coord. Chem. Rev.* **2008**, *252*, 2572. (b) Barbieri, A.; Accorsi, G.; Armaroli, N. *Chem. Commun.* **2008**, 2185. (c) Henry, M.; Wotton, J. L.; Khan, S. I.; Zink, J. I. *Inorg. Chem.* **1997**, *36*, 796. (d) Knorr, M.; Guyon, F.; Khatyr, A.; Däschlein, C.; Strohmann, C.; Aly, S. M.; Abd-El-Aziz, A. S.; Harvey, P. D. *Dalton Trans.* **2009**, 948.
(22) (a) Dexter, D. L. *J. Chem. Phys.* **1953**, *21*, 836. (b) Brown, T. D.; Shepherd, T. M. *J. Chem. Soc., Dalton Trans.* **1973**, 336.

Conclusion

In summary, a new family of novel 3D Ln(III)−Cu(I) coordination polymers has been synthesized hydrothermally. Of particular interest in the mixed ligands pydc and bipy is their propensity to bind Cu(I)−Ln(III) heterometallic ions simultaneously forming a rare spindle-shaped heterometallocycle, which can be viewed as SBUs in the construction of a novel pillared layer open framework. The solid-state luminescent spectra of the compounds **1**−**8** demonstrate that d^{10}-f^n heterometallic coordination polymers may be considered as bifunctional luminescent materials exhibiting strong emitting of either d^{10} or f^n metal ion under excitation of UV rays. The coexistence of d^{10} with f^n metal ions in coordination polymers provides a new route to construct potential photoactive materials with fascinating structures. The studies of the energy transfer process between the d^{10}-f^n heterometallic ions and ligands, together with other gas absorption capabilities, are underway in our laboratory to explore the relationships between the structure and property of these heterometallic coordination polymers. Furthermore, it is believed that the preliminary results presented here may open a promising avenue to rational design of such pillared-layer d^{10}-f^n heterometallic coordination polymers, which not only increase our photochemistry knowledge of these luminescent materials with intriguing architectures, but also lead to new multifunctional materials applicable in molecular adsorption and bimetallic catalysis.

Experimental Section

General Remarks. All the syntheses are performed in poly(tetrafluoroethylene)-lined stainless steel autoclaves under autogenous pressure. Reagents are purchased commercially and are used without further purification. Elemental analyses (C, H, and N) are performed on a Perkin−Elmer 2400 Series II CHNS/O elemental analyzer. Pr, Nd, Sm, Eu, Gd, Tb, Er, Yb, and Cu are determined by Inductively Coupled Plasma (ICP) analysis performed on a Perkin−Elmer Optima 3300DV spectrometer. The shape of the samples was observed with an XP-201 optical microscope. IR spectra were recorded in the range 400−4000 cm^{-1} on a Perkin−Elmer FTIR spectrometer using KBr pellets. TG-DTA analyses are performed on a Perkin-Elmer Diamond TG/DTA Instruments in flowing air with a heating rate of 10 °C min^{-1}. The nitrogen adsorption/desorption isotherms are measured at 77 K using a Micromeritics ASAP 2020 system. Emission spectra are obtained on an Edinburgh Instruments analyzer model FLS920 spectrofluorometer. XRPD patterns of the samples are recorded on an X-ray diffractometer (Rigaku D/Max 2200PC) with a graphite monochromator and $Cu_{K\alpha}$ radiation at room temperature while the voltage and electric current are held at 40 kV and 20 mA. Crystal data of all the compounds are collected on a Bruker SMART APEX CCD-based diffractometer ($Mo_{K\alpha}$ radiation, $\lambda = 0.71073$ Å). The structures are solved by direct methods and refined by a full matrix least-squares technique based on F^2 using the SHELXL 97 program. All of the non-hydrogen atoms were refined anisotropically. The organic hydrogen atoms were generated geometrically; the aqua hydrogen atoms were located from difference maps and refined with isotropic temperature factors. Crystallographic data for the structures reported in this paper have been deposited with the Cambridge Crystallographic Data Centre as supplementary publication no. CCDC-739130 (**1**), CCDC-739129 (**2**), CCDC-739128 (**3**), CCDC-739127 (**4**), CCDC-739126 (**5**), CCDC-739125 (**6**), CCDC-739124 (**7**), and CCDC-739123 (**8**). Copies of the data can be obtained free of charge on application to CCDC, 12 Union Road, Cambridge CB21EZ, U.K. (fax: (+44) 1223−336−033; e-mail: deposit@ccdc.cam.ac.uk).

Preparation. Synthesis of [$Pr(pydc)_3Cu_3(bipy)_3\cdot 5(H_2O)$] (1). A mixture of Pr_6O_{11} (0.3369 g, 0.33 mmol), CuO (0.0795 g, 1.00 mmol), 2,6-pyridinedicarboxylic acid (0.3342 g, 2.00 mmol), 4,4′-bipyridine (0.0469 g, 0.30 mmol), and H_3PO_3 (0.0820 g, 1.00 mmol) in 10 mL of H_2O were stirred for 20 min at room temperature. The mixture was then transferred into a 23 mL, Teflon-lined stainless-steel vessel. The mixture was heated at 160 °C for 3 days under autogenous pressure. After the reaction mixture had slowly cooled down to room temperature, yellowish prism-shaped crystals of **1** were filtered off, washed with distilled water, and dried in air. The crystal is insoluble in water and common organic solvents.

Elemental analysis (%) for C51H43O17 N9Cu3Pr (1385.48): calcd. C 44.21, H 3.13, N 9.10, Cu 13.76, Pr 10.17; found C 44.12, H 3.15, N 9.05, Cu 13.69, Pr 10.09.

IR (KBr pellet, cm^{-1}): 3422 vs, 1623 vs, 1602 w, 1573 w, 1532 w, 1485 m, 1433 s, 1388 vs, 1368 w, 1276 s, 1215 m, 1189 m, 1078 m, 1022 m, 919 m, 813 m, 800 w, 769 m, 728 s, 699 m, 662 m, 568 w, 490 m, 449 w.

Synthesis of [$Nd(pydc)_3Cu_3(bipy)_3\cdot 5(H_2O)$] (2). Synthesis of **2** is similar to that of **1** using Nd_2O_3 (0.3365 g, 1.00 mmol) instead of Pr_6O_{11}. Yellowish prism-shaped crystals of **2** are obtained. The crystal is also insoluble in water and common organic solvents.

Elemental analysis (%) for C51H43O17 N9Cu3Nd (1388.82): calcd. C 44.11, H 3.12, N 9.08, Cu 13.73, Nd 10.39; found C 44.16, H 3.18, N 9.03, Cu 13.70, Nd 10.31.

IR (KBr pellet, cm^{-1}): 3422 vs, 1619 vs, 1573 w, 1532 w, 1485 m, 1431 s, 1384 vs, 1374 w, 1276 s, 1219 m, 1188 m, 1071 m, 1022 m, 916 m, 854 w, 813 m, 803 w, 772 m, 728 s, 697 m, 661 m, 570 w, 492 m, 443 w.

Synthesis of [$Sm(pydc)_3Cu_3(bipy)_3\cdot 4(H_2O)$] (3). Synthesis of **3** is similar to that of **1** using Sm_2O_3 (0.3487 g, 1.00 mmol) instead of Pr_6O_{11}. Yellowish prism-shaped crystals of **3** are obtained. The crystal is also insoluble in water and common organic solvents.

Elemental analysis (%) for C51H41O16 N9Cu3Sm (1376.92): calcd. C 44.49, H 3.00, N 9.16, Cu 13.85, Sm 10.92; found C 44.38, H 3.05, N 9.10, Cu 13.76, Sm 10.85.

IR (KBr pellet, cm^{-1}): 3429 vs, 1623 vs, 1601 w, 1578 m, 1525 w, 1486 m, 1450 w, 1429 s, 1382 vs, 1368 w, 1278 s, 1216 m, 1187 m, 1135 w, 1082 m, 1062 m, 1021 m, 923 m, 860 w, 826 w, 814 s, 770 m, 731 vs, 697 m, 665 m, 568 w, 521 w, 479 m, 437 w.

Synthesis of [$Eu(pydc)_3Cu_3(bipy)_3\cdot 4(H_2O)$] (4). Synthesis of **4** is similar to that of **1** using Eu_2O_3 (0.3519 g, 1.00 mmol) instead of Pr_6O_{11}. Yellowish prism-shaped crystals of **4** are obtained. The crystal is also insoluble in water and common organic solvents.

Elemental analysis (%) for C51H41O16 N9Cu3Eu (1378.52): calcd. C 44.43, H 3.00, N 9.14, Cu 13.83, Eu 11.02; found C 44.34, H 3.02, N 9.09, Cu 13.75, Eu 10.96.

IR (KBr pellet, cm^{-1}): 3429 vs, 1623 vs, 1602 w, 1571 m, 1527 w, 1485 m, 1450 w, 1430 s, 1380 vs, 1366 w, 1275 s, 1215 m, 1188 m, 1130 w, 1080 w, 1060 m, 1020 m, 921 m, 861 w, 823 w, 810 s, 774 m, 732 vs, 699 m, 663 m, 571 w, 525 w, 484 m, 437w.

Synthesis of [$Gd(pydc)_3Cu_3(bipy)_3\cdot 4(H_2O)$] (5). Synthesis of **5** is similar to that of **1** using Gd_2O_3 (0.3625 g, 1.00 mmol) instead of Pr_6O_{11}. Yellowish prism-shaped crystals of **5** are obtained. The crystal is also insoluble in water and common organic solvents.

Elemental analysis (%) for C51H41O16 N9Cu3Gd (1383.81): calcd. C 44.27, H 2.99, N 9.11, Cu 13.78, Gd 11.36; found C 44.20, H 3.01, N 9.07, Cu 13.69, Gd 11.28.

IR (KBr pellet, cm^{-1}): 3432 vs, 1621 vs, 1602 w, 1577 m, 1529 w, 1485 m, 1450 w, 1432 s, 1380 vs, 1369 w, 1278 s, 1218 m, 1187 m, 1141 w, 1080 w, 1061 m, 1022 m, 919 m, 861 w, 825 w, 808 s, 772 m, 729 vs, 693 m, 661 m, 571 w, 523 w, 483 m, 433 w.

Synthesis of [$Tb(pydc)_3Cu_3(bipy)_3\cdot 4(H_2O)$] (6). Synthesis of **6** is similar to that of **1** using Tb_4O_7 (0.3738 g, 0.50 mmol) instead

of Pr_6O_{11}. Yellowish prism-shaped crystals of **6** are obtained. The crystal is also insoluble in water and common organic solvents.

Elemental analysis (%) for C51H41O16 N9Cu3Tb (1385.48): calcd. C 44.21, H 2.98, N 9.10, Cu 13.76, Tb 11.47; found C 44.18, H 3.02, N 9.05, Cu 13.70, Tb 11.36.

IR (KBr pellet, cm^{-1}): 3429 vs, 1624 vs, 1602 w, 1570 m, 1527 w, 1488 m, 1451 w, 1433 s, 1381 vs, 1367 w, 1278 s, 1218 m, 1189 m, 1136 w, 1082 w, 1071 m, 1023 m, 919 m, 861 w, 825 w, 810 s, 770 m, 731 vs, 703 m, 664 m, 572 w, 520 w, 483 m, 436 w.

Synthesis of $[Er(pydc)_3Cu_3(bipy)_3 \cdot 4(H_2O)]$ (7). Synthesis of **7** is similar to that of **1** using Er_2O_3 (0.3825 g, 1.00 mmol) instead of Pr_6O_{11}. Yellowish prism-shaped crystals of **7** are obtained. The crystal is also insoluble in water and common organic solvents.

Elemental analysis (%) for C51H41O16 N9Cu3Er (1393.82): calcd. C 43.95, H 2.96, N 9.04, Cu 13.68, Er 12.00; found C 43.87, H 3.05, N 9.01, Cu 13.62, Er 11.96.

IR (KBr pellet, cm^{-1}): 3422 vs, 1622 vs, 1573 m, 1529 w, 1490 m, 1454 w, 1431 s, 1377 vs, 1370 w, 1281 s, 1221 m, 1190 m, 1139 w, 1082 w, 1069 m, 1022 m, 916 m, 865 w, 828 w, 813 s, 777 m, 730 vs, 697 m, 661 m, 570 w, 523 w, 490 m, 441 w.

Synthesis of $[Yb(pydc)_3Cu_3(bipy)_3 \cdot 4(H_2O)]$ (8). Synthesis of **8** is similar to that of **1** using Yb_2O_3 (0.3941 g, 1.00 mmol) instead of Pr_6O_{11}. Yellowish prism-shaped crystals of **8** are obtained. The crystal is also insoluble in water and common organic solvents.

Elemental analysis (%) for C51H41O16 N9Cu3Yb (1399.60): calcd. C 43.77, H 2.95, N 9.01, Cu 13.62, Yb 12.36; found C 43.71, H 2.99, N 8.97, Cu 13.56, Yb 12.32.

IR (KBr pellet, cm^{-1}): 3422 vs, 1622 vs, 1575 m, 1532 w, 1488 m, 1457 w, 1433 s, 1377 vs, 1369 w, 1281 s, 1219 m, 1190 m, 1139 w, 1079 w, 1069 m, 1022 m, 919 m, 857 w, 831 w, 813 s, 800 w, 774 m, 730 vs, 697 m, 660 m, 570 w, 526 w, 490 m, 443 w.

Acknowledgment. Financial support from the Key Subject (Laboratory) Research Foundation of Shandong Province is gratefully acknowledged. The authors wish to thank professor I. D. Brown for providing the computer software of the Bond Valence Calculator and Walter Rogers for emendating the English usage.

Supporting Information Available: X-ray crystallographic data in CIF format, hydrogen bonds, Bond Valence Sums, perspective view of $[Ln_6(pydc)_6Cu_{12}(bipy)_6]$ basic building block and its corrugated linkage, wiew of the lanthanide pseudohexagon in a chair form, FT-IR spectra, and so forth. This material is available free of charge via the Internet at http://pubs.acs.org.